

LETTER • OPEN ACCESS

Improved spatial representation of a highly resolved emission inventory in China: evidence from TROPOMI measurements

To cite this article: Nana Wu *et al* 2021 *Environ. Res. Lett.* **16** 084056

View the [article online](#) for updates and enhancements.

ENVIRONMENTAL RESEARCH
LETTERS

LETTER

OPEN ACCESS

RECEIVED
8 June 2021REVISED
13 July 2021ACCEPTED FOR PUBLICATION
23 July 2021PUBLISHED
5 August 2021

Original content from
this work may be used
under the terms of the
[Creative Commons
Attribution 4.0 licence](#).

Any further distribution
of this work must
maintain attribution to
the author(s) and the title
of the work, journal
citation and DOI.



Improved spatial representation of a highly resolved emission inventory in China: evidence from TROPOMI measurements

Nana Wu¹, Guannan Geng^{2,*} , Liu Yan¹, Jianzhao Bi¹, Yanshun Li¹, Dan Tong¹, Bo Zheng³ 
and Qiang Zhang¹¹ Ministry of Education Key Laboratory for Earth System Modelling, Department of Earth System Science, Tsinghua University, Beijing 100084, People's Republic of China² State Key Joint Laboratory of Environment Simulation and Pollution Control, School of Environment, Tsinghua University, Beijing 100084, People's Republic of China³ Institute of Environment and Ecology, Tsinghua Shenzhen International Graduate School, Tsinghua University, Shenzhen 518055, People's Republic of China

* Author to whom any correspondence should be addressed.

E-mail: guannangeng@tsinghua.edu.cn**Keywords:** emission inventory, high-resolution, TROPOMISupplementary material for this article is available [online](#)**Abstract**

Emissions in many sources are estimated in municipal district totals and spatially disaggregated onto grid cells using empirically selected spatial proxies such as population density, which might introduce biases, especially in fine spatial scale. Efforts have been made to improve the spatial representation of emission inventory, by incorporating comprehensive point source database (e.g. power plants, industrial facilities) in emission estimates. Satellite-based observations from the Tropospheric Monitoring Instrument (TROPOMI) with unprecedented pixel sizes ($3.5 \times 7 \text{ km}^2$) and signal-to-noise ratios offer the opportunity to evaluate the spatial accuracy of such highly resolved emissions from space. Here, we compare the city-level NO_x emissions from a proxy-based emission inventory named the Multi-resolution Emission Inventory for China (MEIC) with a highly resolved emission inventory named the Multi-resolution Emission Inventory for China - High Resolution (MEIC-HR) that has nearly 100 000 industrial facilities, and evaluate them through NO_x emissions derived from the TROPOMI NO_2 tropospheric vertical column densities (TVCDs). We find that the discrepancies in city-level NO_x emissions between MEIC and MEIC-HR are influenced by the proportions of emissions from point sources and NO_x emissions per industrial gross domestic product (IGDP). The use of IGDP as a spatial proxy to disaggregate industrial emissions tends to overestimate NO_x emissions in cities with lower industrial emission intensities or less industrial facilities in the MEIC. The NO_x emissions of 70 cities are derived from one year TROPOMI NO_2 TVCDs using the exponentially modified Gaussian function. Compared to the satellite-derived emissions, the cities with higher industrial point source emission proportions in MEIC-HR agree better with space-constrained results, indicating that integrating more point sources in the inventory would improve the spatial accuracy of emissions on city scale. In the future, we should devote more efforts to incorporating accurate locations of emitting facilities to reduce uncertainties in fine-scale emission estimates and guide future policies.

1. Introduction

Emission inventories have played an essential role in atmospheric science research and air quality management, as they could support air pollution modeling and forecasting, formulating emission

mitigation policies and assessing their effects. Emissions are fundamental inputs for chemical transport models (CTMs), and their spatial patterns are an important factor that determines the model performance, especially at fine resolutions. Therefore, it is particularly critical to

evaluate the spatial representations of emission inventories.

The traditional and widely used method to develop an emission inventory is the proxy-based method, which estimates emission totals at the municipal level (e.g. countries or provinces) and allocates them to fine grids using spatial proxies (e.g. population density, nighttime light, road networks) [1–6]. The proxy-based method is based on an assumption that emissions are linearly correlated with the selected proxies, which might introduce biases since the energy consumption and emission level per unit of proxies are spatially heterogeneous [7–13]. Previous studies have shown that high-resolution ($<0.25^\circ$) emissions generated from the proxy-based method tend to overestimate emissions in urban areas and underestimate emissions in suburban and rural regions [14]. Such biases were also found to propagate into uncertainties in high-resolution CTMs [15–19].

In the past few years, extensive and detailed bottom-up information supports the development of highly resolved emission inventories [14, 16–18, 20–24], especially for the industrial sector. Emissions are estimated at the factory or even unit level, involving unit-specific activity data, emission factors and pollution removal efficiencies [14, 16–18, 20–24]. These data are distributed to fine grids in the form of point sources using exact geographical coordinates instead of spatial proxies, which allows emission disaggregation to high spatial resolution (1×1 km) [18]. Recent efforts indicate that estimating emissions from point sources exhibit better agreements with satellite observations [15, 24] and surface observations [14, 16, 18]. Sensitivity analysis through CTMs suggests that spatial biases are reduced significantly as the point source shares increase [14]. However, the discrepancies in the city-level emissions between proxy-based and highly resolved emission inventories have rarely been studied and evaluated. Direct evaluation of emissions against independent data sources are needed.

In recent years, satellite remote sensing has become an important tool to validate emission inventories because of its high spatial resolution and wide spatial-temporal coverage. High-resolution measurements (e.g. the Ozone Monitoring Instrument, OMI) provide an independent way to quantify emissions through Gaussian models [25–31], eliminating the need for CTMs and priori emission inventories. Beirle *et al* [25] simultaneously derived the NO_x lifetimes and emissions of isolated megacities by means of the downwind evolution of OMINO_2 in different wind directions, which was subsequently modified by Liu *et al* [28] to be applied to polluted areas [24, 30, 31]. With the launch of the Tropospheric Monitoring Instrument (TROPOMI) in 2017 [32], data with unprecedented pixel sizes (3.5×7 km²) and signal-to-noise ratios made it possible to resolve plumes with even only one overpass [33, 34]. Unlike

the long-term (one year or more) OMI data required for NO_x estimates, seasonal or subseasonal TROPOMI data are capable of quantifying NO_x emissions, and under extremely special conditions, even data from a single day are sufficient [34]. Beirle *et al* [33] has demonstrated that NO_x emissions from large point sources can be mapped at high spatial resolution based on TROPOMI measurements and the continuity equation.

In this work, we first compare the city-level NO_x emissions from a proxy-based emission inventory and a highly resolved emission inventory that contains nearly 100 000 industrial infrastructures over China to study their differences and related impact factors. We investigate how point source shares influence emission allocations from provinces to cities under the premise of equal emissions at the province level. Then we use TROPOMI NO_2 tropospheric vertical column densities (TVCDs) and the exponentially modified Gaussian (EMG) function to derive NO_x emissions from Chinese cities. Finally, the city-level NO_x emissions from the two emission inventories are evaluated using the satellite-derived NO_x emissions.

2. Data and methods

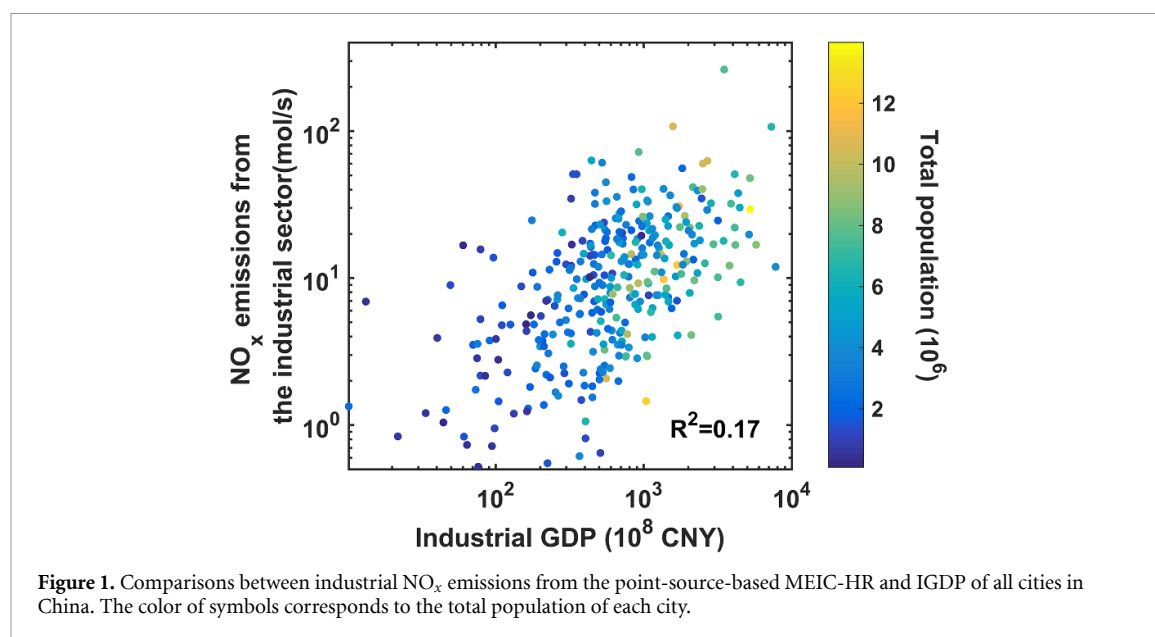
2.1. Emission inventories

The proxy-based emission inventory evaluated in this work is obtained from the Multi-resolution Emission Inventory for China (MEIC, www.meicmodel.org) [35, 36] for the year 2017. In MEIC, only the coal-fired power sector is estimated as point sources based on unit-level data [14, 21], while other sectors such as industry, transportation and residential are regarded as mobile or area sources. The highly resolved emission inventory used here is the Multi-resolution Emission Inventory for China - High Resolution (MEIC-HR), which was compiled by Zheng *et al* [18] and subsequently updated from 2013 to 2017. The MEIC-HR is built under the framework of MEIC but contains a large number of industrial point sources (i.e. nearly 100 000 industrial facilities). Factory- or facility-level information is combined from three industrial datasets to estimate emissions for each industrial facility. More details about the input datasets and the data processing for MEIC-HR can be found in Zheng *et al* [18].

The magnitudes of the NO_x emissions for each sector are the same at the province level in MEIC and MEIC-HR (table 1), which ensures that the city-level emission discrepancies between these two inventories result only from spatial allocations rather than emission magnitudes. As shown in table 1, anthropogenic NO_x emissions from all sectors in 2017 is 20.08 Tg, of which 37% are industrial emissions. Four industrial subsectors (i.e. boiler, iron, cement and glass) apply different emission allocation methods between MEIC and MEIC-HR: the MEIC relies on the county-level industrial gross domestic product

Table 1. The emission allocation methods from provinces to cities in different sectors in MEIC-HR and MEIC. Emission magnitudes and emission proportions by sector are also listed. The bold font represents the discrepancies between MEIC-HR and MEIC.

Sector	Subsector	Province to city		Emissions (Tg)	Proportion
		MEIC-HR	MEIC		
Industry	Boiler	Point source	Industrial GDP	2.66	13%
	Iron	Point source		2.49	12%
	Cement	Point source		0.92	5%
	Glass	Point source		0.31	2%
	Other industry		Industrial GDP	0.99	5%
Power	—		Point source	4.14	21%
Residential	—		Urban population/Rural population	0.85	4%
Transportation	On-road		Vehicle population	7.72	38%
	Off-road		Machine power/Total GDP/population		



(IGDP), while the MEIC-HR is mapped based on the exact locations of the industrial facilities. We define a variable as industrial point source emission proportions (i.e. industrial PS proportions), which represents the ratio of point-based emissions from boiler, iron, cement and glass in the MEIC-HR to emissions from all sectors. Although emissions from the power sector are also point sources, they are exactly the same in the two emission inventories and are not considered in the point source proportion calculation, as we mainly focus on the differences brought by the four industrial subsectors. Emission disaggregation for other industry, power, residential and transportation in MEIC and MEIC-HR are the same.

Although population and IGDP are widely utilized in spatial allocations, it is worth noting that city-level NO_x emissions from industrial sectors are not linearly correlated with IGDP (figure 1). IGDP data and population data used in this study are from China City Statistical Yearbook 2017 [37]. The R^2 between industrial NO_x emissions and IGDP is 0.17, and the R^2 between NO_x emissions from the industrial sector and the total population is as low as 0.07. As a

consequence, uncertainties caused by the linear hypothesis in proxy-based methods need to be evaluated.

2.2. Satellite and wind data

TROPOMI is a payload on Sentinel-5 Precursor (S5P), which was launched on 13 October 2017 by the European Space Agency. The instrument achieves daily global coverage with a swath width of 2600 km and ascends across the equator at approximately 13:30 local time. Compared to OMI, the significant improvements of TROPOMI are unparalleled spatial resolution of up to $3.5 \times 7 \text{ km}^2$ (upgraded to $5.5 \times 3.5 \text{ km}^2$ on 6 August 2019) and 1–5 times higher signal-to-noise ratios, which provide more details on a fine scale and improve the quality and reliability of the captured data. NO₂ is one of the main trace gases measured by TROPOMI, of which NO₂ processor realizes many retrieval improvements [38].

In this study, we use NO₂ TVCDs over China from February 2018 to February 2019 from the official TM5-MP-DOMINO version 1.0.0 L2 offline product (www.temis.nl/airpollution/no2col/data/tropomi/). Pixels with ‘quality assurance value’ below

0.75 are filtered to remove cloud radiance fraction greater than 0.5 and erroneous retrievals [38]; then, NO₂ TVCDs are mapped at 0.06° × 0.06°. Wind fields below 500 m with 0.36 degrees spatial resolution and six-hour temporal resolution are taken from the ECMWF reanalysis (www.ecmwf.int/en/research/climate-reanalysis/era-interim). Following the method described in Liu *et al* [28], the six hourly ECMWF wind fields are interpolated in time to match TROPOMI overpass time, and horizontal wind components are averaged in the vertical direction according to the weight of the layer height.

2.3. Fitting the NO_x emissions and lifetimes of cities

The EMG model is used to derive the NO_x emissions and atmospheric lifetimes of cities following the method developed by Liu *et al* [28], which is for sources located in a heterogeneously polluted background and applicable to our work. Wind fields are divided into calm and windy conditions with a threshold of 2 m s⁻¹, as in Beirle *et al* [25] and Liu *et al* [28]. The NO₂ spatial distributions under calm conditions represent the spatial patterns of NO_x emissions. Changes in the NO₂ spatial patterns from calm to windy conditions indicate how long NO₂ survives in the atmosphere. The function for the lifetime fit is expressed as follows:

$$N(x) = a \times [e \otimes C](x) + b \quad (1)$$

$$e(x) = \exp\left(-\frac{x}{x_0}\right) \quad (2)$$

$$\tau = \frac{x_0}{w} \quad (3)$$

where $N(x)$ represents a model function for the observed NO₂ line densities (i.e. NO₂ per cm), which are calculated by integration of the mean NO₂ TVCDs perpendicular to the wind direction. The removal of NO₂ can be simply described by a first order loss and thus the truncated exponential decay function $e(x)$ represents the chemical decay of NO₂. $C(x)$ represents the NO₂ patterns under calm conditions, and a, b reflect systematic deviations between windy and calm wind, x_0 is the e-folding distance downwind, w is the mean wind speed. A nonlinear least-squares fit of $N(x)$ is performed to derive a, b and x_0 , and the e-folding distance x_0 is divided by the average wind speed w to obtain the lifetime τ .

The emission rate is obtained in three steps according to the mass balance (equation (4)). First, the total NO₂ mass A_{NO_2} under calm conditions around the centers of emitting sources are quantified (equation (5)). We use a corrected factor $f(\sigma_i)$ based on the fitted width of the Gaussian plume to scale A_{NO_2} to account for possible losses by cross-wind dilution as Liu *et al* [28] do (see equation (6)). Then NO₂ is converted to NO_x with a conversion coefficient of 1.32, as suggested by Beirle *et al* [25] and Liu *et al* [28]. Finally, the NO_x mass A_{NO_x} is divided by the corresponding lifetime τ to obtain NO_x emission rates (equation (4)). The most complicated part of the above processes is the calculation of the total NO₂ mass under calm conditions, and the fitting model is as equation (5):

$$E = \frac{A_{\text{NO}_x}}{\tau} \quad (4)$$

$$g_i(x) = A_{\text{NO}_2} \times \frac{1}{\sqrt{2\pi}\sigma_i} \exp\left(-\frac{(x-X)^2}{2\sigma_i^2}\right) + \varepsilon_i + \beta_i x \quad (5)$$

$$f(\sigma_i) = \int_{-20\text{km}}^{20\text{km}} \frac{1}{\sqrt{2\pi}\sigma_i} \exp\left(-\frac{(x-X)^2}{2\sigma_i^2}\right) \Bigg/ \int_{-\infty}^{\infty} \frac{1}{\sqrt{2\pi}\sigma_i} \exp\left(-\frac{(x-X)^2}{2\sigma_i^2}\right) \quad (6)$$

where $g(x)$ is a modified Gaussian function, which is for NO₂ line densities (i.e. NO₂ per cm) under calm wind, i represents the wind directions of rotation, A_{NO_x} and A_{NO_2} are the NO_x amount and NO₂ amount, respectively, X is the location of inversion sites, ε_i and β_i indicate the hypothesis of a linear distribution of background concentrations, and σ_i represents the standard deviation of $g(x)$.

We apply nonlinear least-squares fitting methods to calculate the lifetimes and emissions of cities. In accordance with the set in Liu *et al* [28], we

use 600 km as the fitting interval and 300 km as the integration interval for lifetime fit, and we set a fitting interval of 200 km (300 km for Pearl River Delta) and an integration interval of 40 km (60 km for Pearl River Delta) for total NO₂ mass fit. Strict constraints are set on fit performance, as shown in Liu *et al* [28]: $R \geq 0.9$, confidence intervals of lifetime < 10 h, confidence intervals of the NO₂ amount ≤ 0.8 times of itself, lower bound of confidence intervals > 0. The fitting model shows robust ability to derive the lifetimes and emissions of cities. Uncertainties resulting from the parameters used in the model

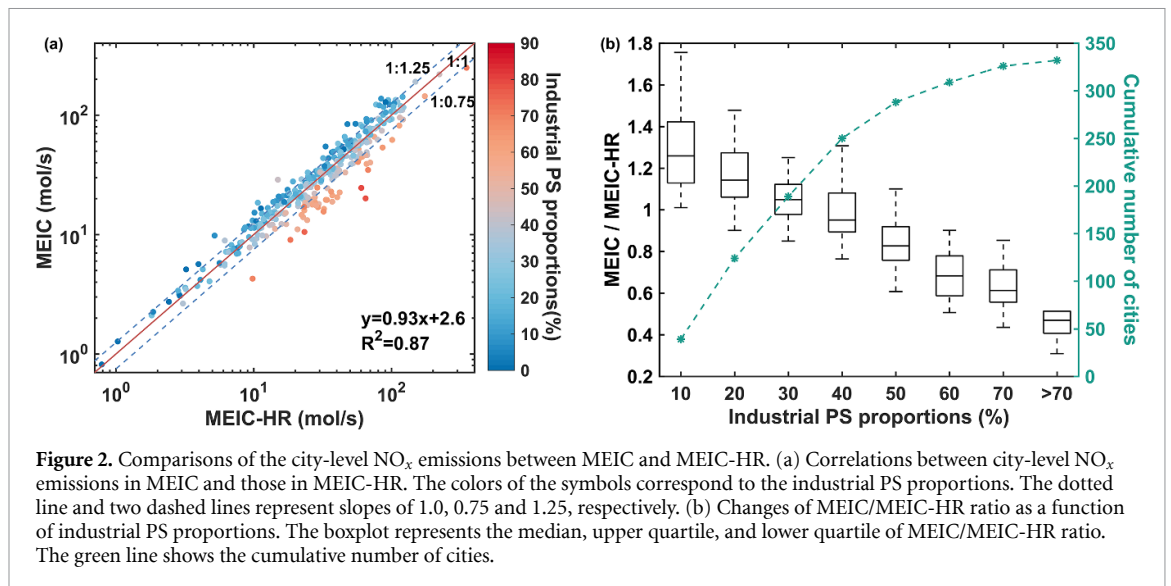


Figure 2. Comparisons of the city-level NO_x emissions between MEIC and MEIC-HR. (a) Correlations between city-level NO_x emissions in MEIC and those in MEIC-HR. The colors of the symbols correspond to the industrial PS proportions. The dotted line and two dashed lines represent slopes of 1.0, 0.75 and 1.25, respectively. (b) Changes of MEIC/MEIC-HR ratio as a function of industrial PS proportions. The boxplot represents the median, upper quartile, and lower quartile of MEIC/MEIC-HR ratio. The green line shows the cumulative number of cities.

and other factors for the lifetime and emission fit are presented in section 4.1. In addition, sites with an elevation difference of more than 250 m in ECMWF and GTOPO30 (<https://earthexplorer.usgs.gov/>) are defined as mountainous cities and eliminated in our analysis, as in Liu *et al* [28].

3. Results

3.1. City-level NO_x emissions in the two emission inventories

Figure 2(a) compares the city-level NO_x emissions from MEIC and MEIC-HR. Although the R^2 value reaches 0.87, most cities deviate from the 1:1 line, among which 96 cities deviate by more than 25%, accounting for approximately 39% of the total cities. This result indicates that different spatial disaggregation methods lead to city-level emission discrepancies considering that provincial NO_x emissions in MEIC and MEIC-HR are the same. The differences between city-level NO_x emissions in MEIC and MEIC-HR are related to the industrial PS proportions in each city, with cities of high industrial PS proportions below the 1:1 line and vice versa. Figure 2(b) further analyzes the ratio of NO_x emissions in the MEIC to those in the MEIC-HR (MEIC/MEIC-HR) as a function of industrial PS proportions. The MEIC/MEIC-HR ratio decreases with the median value from 1.26 to 0.47 as the industrial PS proportions increase from 10% to more than 70%, indicating that the proxy-based inventory (MEIC) tends to overestimate the NO_x emissions for cities with lower industrial PS proportions and underestimate the NO_x emissions for cities occupied by a large amount of industrial factories (i.e. higher industrial PS proportions).

In the MEIC, IGDP is used as the spatial proxy to allocate industrial NO_x emissions from province level to cities/counties, which may induce biases since NO_x emissions per IGDP are heterogeneous among

regions. Figure 3 presents the discrepancies of city-level NO_x emissions between MEIC and MEIC-HR and their relationships with IGDP and industrial PS proportions in each city. In a certain industrial PS proportion range, the average MEIC/MEIC-HR ratio decreases along with the increase in NO_x emissions per IGDP. For example, when industrial PS proportions are less than 10%, the average MEIC/MEIC-HR ratio declines from 1.38 to 1.07 as the NO_x emissions per IGDP increase from 35 to over 140 t/10⁸ CNY. Compared to the real-world emissions, the assumption that NO_x emissions are linearly associated with IGDP tends to allocate more/less emissions to cities with low/high emission intensities, which results in overestimation/underestimation of NO_x emissions in the MEIC. Similarly, in a certain range of NO_x emissions per IGDP, the average MEIC/MEIC-HR ratio decreases as industrial PS proportions increase. For example, when the NO_x emissions per IGDP are between 35 and 70 t/10⁸ CNY, the average MEIC/MEIC-HR decreases from 1.28 to 0.65 as industrial PS proportions increase from 10% to over 70%. As the industrial PS proportions defined in our study are from highly polluting industries such as iron and cement, lower industrial PS proportions under a certain range of emission intensity reflect that the IGDP in those cities are contributed more by other cleaning industries. Therefore, using IGDP to allocate emissions from province level to cities tend to overestimate the industrial emissions of such cities.

3.2. City-level NO_x emissions derived from satellite observations

We apply the EMG model described in section 2.3 and finally derive the NO_x lifetimes and emissions of 70 cities in China from TROPOMI measurements (table S1 (available online at stacks.iop.org/ERL/16/084056/mmedia)). High spatial resolution and low noise enable TROPOMI to have more effective pixels

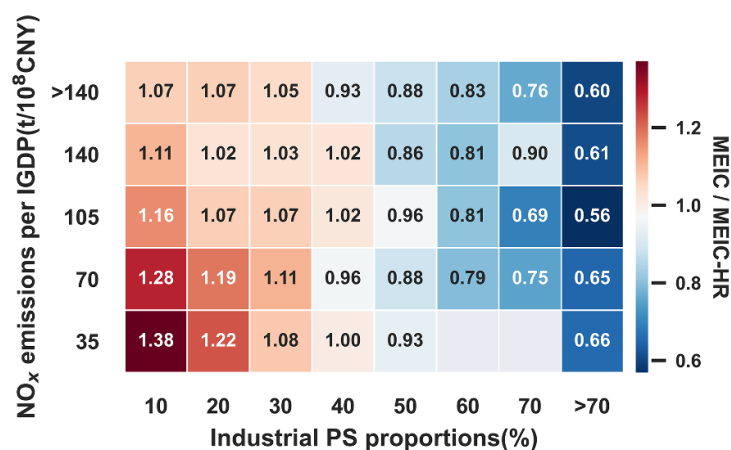


Figure 3. The relationships of MEIC/MEIC-HR ratio with NO_x emissions per IGDP and industrial PS proportions in each city.

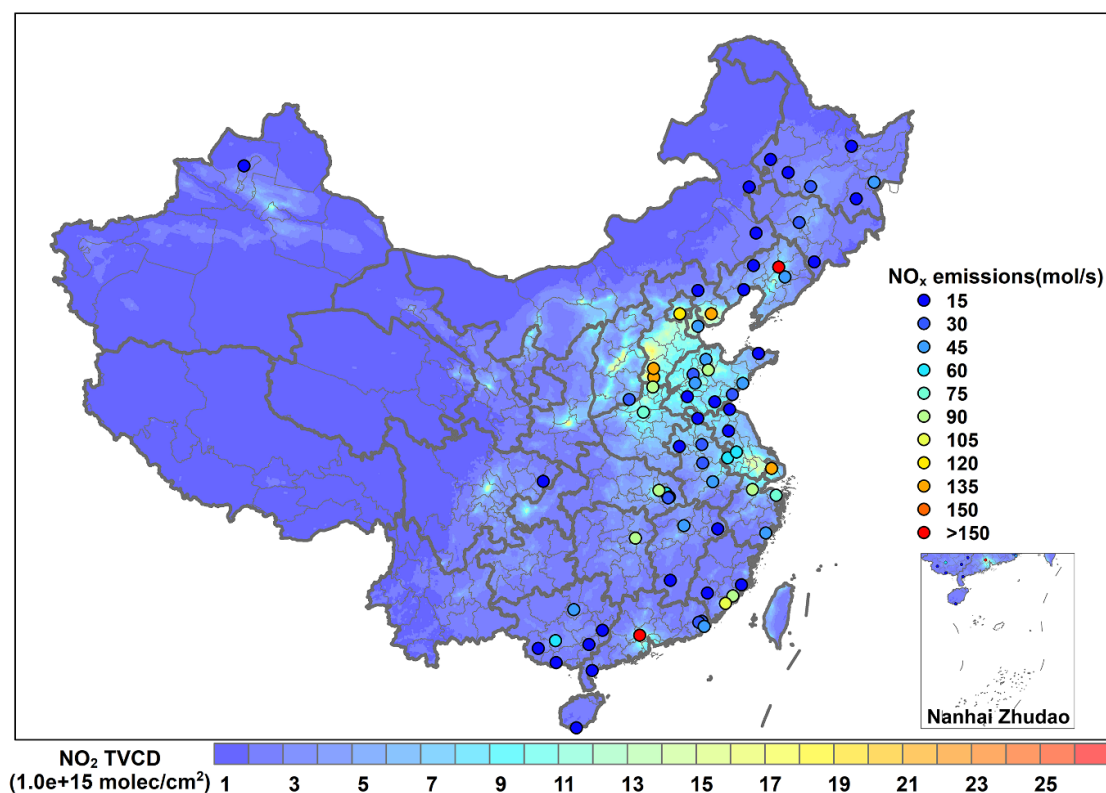
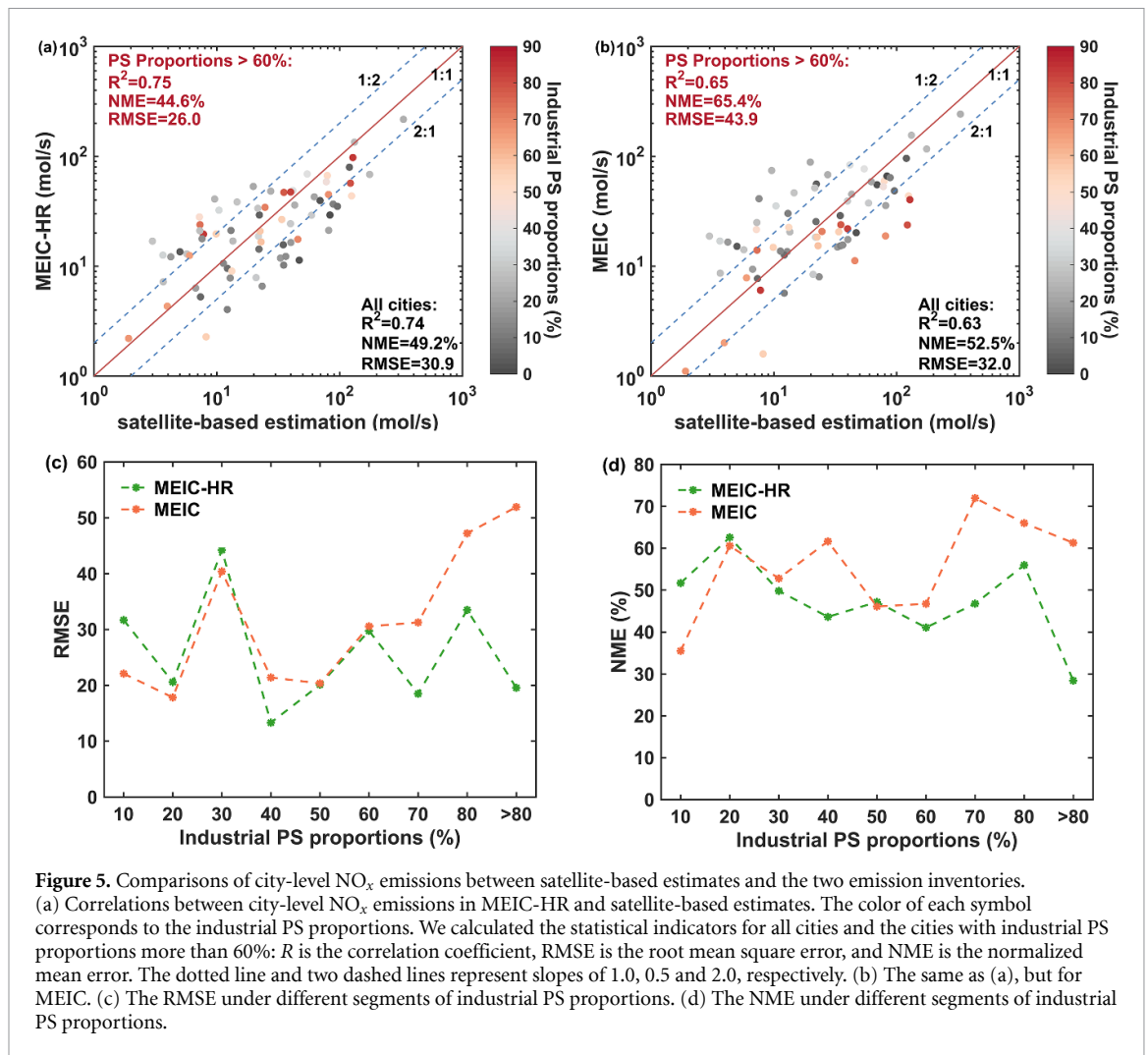


Figure 4. Average TROPOMI NO₂ TVCDs over China from February 2018 to February 2019 overlaid with the locations of cities with successfully derived emissions in this work, and their colors indicate the derived NO_x emissions.

and exhibits a significantly better performance of representing spatial variability than any instrument before it [39, 40], which increases the possibility of meeting the constraints on model performance (see the last paragraph of section 2.3 for details). As the key for deriving NO_x lifetimes and emissions is to ensure strong gradients of the NO₂ signal around the source, the improved estimation of NO_x lifetimes and emissions by high-quality satellite measurements is directly reflected in the greater number of derived cities compared to previous works [28].

The fitted NO_x lifetimes range from 1.0 h to 9.3 h in this work, which correspond to the results reported in the literature [24–26, 28]. The city with the highest NO_x emissions rate is Pearl River Delta (up to 331 mol s⁻¹), while the lowest is Wuzhou (only 2 mol s⁻¹). Figure 4 presents the spatial distributions of the average NO₂ TVCDs over China from February 2018 to February 2019 overlaid with the derived NO_x emissions of 70 cities. Hotspots of average NO₂ TVCDs are mainly located in the North China Plain, Yangtze River Delta, Pearl River Delta, Fenwei Plain



and Sichuan-Chongqing region, which are consistent with the spatial patterns of NO_x emissions of the investigated cities in this study.

3.3. Evaluation through satellite-based NO_x emissions

To evaluate the representations of city-level NO_x emissions in MEIC and MEIC-HR through satellite-based estimates, emissions in the two emission inventories are summed over an area of 40×40 km around the center of the investigated sites, in accordance with the integration interval used in the model functions for NO_2 total mass. Figures 5(a) and (b) show comparisons between the NO_x emissions of 70 cities derived from TROPOMI NO_2 TVCDs and those from the two emission inventories. City-level NO_x emissions in MEIC-HR ($r^2 = 0.74$) show better agreement with satellite-based estimates than those in MEIC ($r^2 = 0.63$). The improvements are related to industrial PS proportions: for cities with high industrial PS proportions (>60%), the root mean square error (RMSE) is 26.0 and 43.9 mol s^{-1} for MEIC-HR and MEIC, respectively, and the normalized mean error (NME) is 44.6% and 65.4%, respectively.

Figures 5(c) and (d) further show a comparison between NO_x emissions in emission inventories and satellite-based estimates as a function of industrial PS proportions. When industrial PS proportions are relatively low (<40%), the performance of MEIC-HR and MEIC is comparable because the NO_x emissions of cities in MEIC-HR and MEIC are close to each other (section 3.1). As point source emission proportions increase from 40% to over 80%, the RMSE and NME of MEIC-HR are always lower than those of MEIC in the same segments of industrial PS proportions, and the gap between them widens gradually. The results indicate that with the increase in industrial PS proportions, the improvement of spatial representations by bottom-up methods becomes increasingly more distinct than those by proxy-based methods. Because real-world emissions are more disproportionate to the IGDP for cities with high point source emission proportions, greater deviations in emissions introduced by the linear assumption in the proxy-based method are produced. Consequently, the highly resolved emission inventories have better spatial representations of real-world emission distributions than proxy-based inventories, especially in regions with a large amount of emitting facilities. It

is crucial to raise point source emission proportions in emission inventories to reduce spatial biases caused by spatial proxies.

4. Discussion

4.1. Uncertainties

There are several uncertainties in this work. Liu *et al* [28] systematically evaluated the uncertainties in the EMG model. Here, following Liu *et al* [28], we estimate the uncertainties of the NO_x lifetimes and emissions from six aspects: (a) sensitivity tests are conducted to quantify the uncertainties from the choice of fit and integration intervals. The fitted lifetimes and emissions are found to be insensitive to the choice of the fit and integration intervals. Table S2 shows that for the lifetime fit, every 100 km changes of the fit interval f or integration interval i cause lifetimes to vary by about 10%. For the total NO₂ mass fit, 10% or 20% changes of the fit interval h or integration interval v lead to less than 20% changes of NO_x emission rates. (b) The 95% confidence interval and the standard mean error of the lifetimes under different wind directions are used to quantify the fit errors for each investigated site. (c) With the consideration of the height of wind fields and threshold for calm winds, the wind fields from ECMWF lead to an uncertainty of ~30% for non-mountainous cities. (d) In this study, we use a constant scaling factor of 1.32 to convert NO₂ to NO_x, which is a typical value under cloud-free conditions around noon when polluted air masses support the formation of O₃ (i.e. TROPOMI overpass time). Although the difference in O₃ concentrations between upwind and downwind plumes might influence NO_x/NO₂, the effect has been included in the overall uncertainty estimates as we average the fit results for different wind direction sectors, which usually represent different incoming O₃ concentrations. The constant NO_x/NO₂ scaling factor brings an uncertainty of ~10% to the derived emissions (but not lifetimes) based on previous studies [25, 28, 31, 33]. (e) The uncertainty of TVCDs is ~30% according to previous studies [39, 41–43], which directly propagates to NO₂ amount and thus the estimated emissions (but not lifetimes). The uncertainty of TVCDs consists of additive and multiplicative terms. The uncertainty of multiplicative terms comes from tropospheric air-mass factor, which depends on profile shape, cloud parameters, albedo and surface pressure [44]. And the uncertainty of TVCDs from additive components owing to the spectral retrieval and stratospheric correction is eliminated by the fitted background in our study. (f) The wind speed is an important impact factor for the fitted lifetime [26], which is assumed to be the same under calm and windy conditions in this work. The systematic difference of NO₂ TVCDs between calm and windy conditions is about 20% (figure S1). We take the factors mentioned above into

consideration and conclude that the total uncertainties of lifetimes and emissions are within 42%–91% and 57%–99%, respectively. This uncertainty range is comparable to Liu *et al* [28] and Liu *et al* [31]. As illustrated in Liu *et al* [28] and Liu *et al* [31], under the assumption that all uncertain factors are independent, the total uncertainty calculated here is rather conservative.

4.2. Implications

In this study, we use NO_x emissions derived from TROPOMI NO₂ TVCDs to evaluate the NO_x emissions on city scale estimated from two bottom-up emission inventories. NO_x is selected as an example here because the errors in NO₂ satellite retrievals are relatively small [41, 45, 46] and the method to derive NO_x emissions in cities from satellite data is solid [25, 28, 31, 34, 47]. The findings obtained in this work that raising point emission proportions in emission inventory could improve its spatial representation on city scale are also applicable to other air pollutant species (e.g. CO₂ and SO₂) from fossil fuel combustion, as they come from the same emission sources.

Recently, some studies have emphasized the importance of spatial allocation method in the development of gridded emissions [7, 14–16, 18, 19]. For example, Zheng *et al* [18] compile the MEIC-HR inventory with comprehensive industrial-facility-level information and find that the point-source-based emission inventory substantially improves the WRF/CMAQ model simulations at high spatial resolution of 4 km compared to the proxy-based emissions. Our study adds new evidence from space to prove the accuracy of the spatial patterns represented by such highly resolved emission inventory. However, due to the limitation of the emission retrieval method, only 70 cities are covered in our evaluation analysis. A more comprehensive evaluation in the future might be comparing modeled tropospheric vertical columns from CTMs at fine spatial resolution with TVCDs with unprecedented resolution from TROPOMI, following the method in Geng *et al* [15].

As reported in previous studies [11, 14, 16–18], emissions from point sources exhibit inconsistent spatial patterns with those from spatial proxies (e.g. population density) at fine spatial scale, which means the decoupling effect between emission inventory constructed from large point database and spatial proxies. More importantly, the spatial patterns of such highly resolved inventory cannot be reproduced by any spatial proxies that have been frequently used before. Therefore, it is crucial to increase the share of point source emissions by including more detailed point source statistical data [11, 14, 16–18], conducting field surveys [17, 24, 48] or identifying missing point sources by means of satellite observations [29, 49, 50]. For example, three industrial datasets are combined in MEIC-HR to

provide a synthesized facility-level database [18]. To develop high-resolution emission inventory, on-site surveys for industrial sources are conducted to obtain key parameters relevant to emission estimation [17, 24, 48]. Owing to the wide spatial coverage, high temporal and spatial resolution, and timely updates, satellite data can be used to detect emission sources including those that are not captured in bottom-up emission inventories due to lack of available data, especially in developing nations. Mclinden *et al* [29] use the measurement of SO₂ from OMI and find nearly 40 emission sources missing from conventional inventories, accounting for roughly 6%–12% of the global anthropogenic source. The combination of bottom-up and top-down information might lead to greater accuracy of fine scale emission inventory in the future.

5. Conclusion

The proxy-based method to allocate emission totals to smaller administrative districts or grids might introduce biases, especially at fine scales. Developing highly resolved emission inventories is an effective way to support fine-scale emission characterization, whose improvement to the spatial representations of emissions needs to be studied. In this work, we evaluate the effect of integrating a large amount of point sources on emission allocations from province level to cities using a proxy-based emission inventory (MEIC), a highly resolved emission inventory (MEIC-HR), and satellite observations. We first investigate the discrepancies in city-level NO_x emissions between the two emission inventories and diagnose the related impact factors. City-level NO_x emissions derived from TROPOMI NO₂ TVCDs are then applied to evaluate the spatial representations of city-level emissions by MEIC and MEIC-HR.

We find that the discrepancies in city-level NO_x emissions between MEIC and MEIC-HR are affected by the industrial PS proportions and NO_x emissions per IGDP. As the industrial PS proportions increase from 10% to over 70%, the median value of MEIC/MEIC-HR ratio decreases from 1.26 to 0.47. When NO_x emissions per IGDP are in a certain range, the mean MEIC/MEIC-HR ratio decreases along with the increase of industrial PS proportions. Similarly, in a certain range of industrial PS proportions, the mean MEIC/MEIC-HR ratio declines as NO_x emissions per IGDP increase. Therefore, Using IGDP as a spatial proxy to allocate provincial industrial NO_x emissions to cities tends to overestimate emissions in cities with lower industrial PS proportions (a less amount of industrial facilities or lower industrial emission intensities). NO_x emissions of 70 cities are derived based on TROPOMI NO₂ TVCDs and the EMG model and applied to evaluate the spatial accuracy of the two emission inventories. City-level NO_x emissions in MEIC-HR ($r^2 = 0.74$) show

better agreement with satellite-based estimates than those in MEIC ($r^2 = 0.63$). And the improvement is more obvious for cities with high industrial PS proportions (>60%), which is manifested as the RMSE is 26.0 and 43.9 mol s⁻¹ for MEIC-HR and MEIC, respectively, and the NME is 44.6% and 65.4% for MEIC-HR and MEIC, respectively, indicating that incorporating comprehensive point source database will improve the spatial representation of emission inventories.

This work emphasizes the importance of integrating more point sources in emission inventories to improve the spatial accuracy. Our study provides a framework to propagate top-down information from satellite to the evaluations of bottom-up inventories, which could support the development and refinement of highly resolved emission inventories in the future. More efforts should be made to develop highly resolved emission inventories to facilitate atmospheric research and air quality management.

Data availability statement

The data that support the findings of this study are available upon reasonable request from the authors.

Acknowledgments

This work was supported by the National Natural Science Foundation of China (91744310 and 42005135).

ORCID iDs

Guannan Geng  <https://orcid.org/0000-0002-1605-8448>

Bo Zheng  <https://orcid.org/0000-0001-8344-3445>

References

- [1] Streets D G *et al* 2003 An inventory of gaseous and primary aerosol emissions in Asia in the year 2000 *J. Geophys. Res. Atmos.* **108** 8809
- [2] Shi K, Chen Y, Yu B, Xu T, Chen Z, Liu R, Li L and Wu J 2016 Modeling spatiotemporal CO₂ (carbon dioxide) emission dynamics in China from DMS-OLS nighttime stable light data using panel data analysis *Appl. Energy* **168** 523–33
- [3] Li M *et al* 2017 MIX: a mosaic Asian anthropogenic emission inventory under the international collaboration framework of the MICS-Asia and HTAP *Atmos. Chem. Phys.* **17** 935–63
- [4] Zheng B, Huo H, Zhang Q, Yao Z L, Wang X T, Yang X F, Liu H and He K B 2014 High-resolution mapping of vehicle emissions in China in 2008 *Atmos. Chem. Phys.* **14** 9787–805
- [5] Zhang Q *et al* 2009 Asian emissions in 2006 for the NASA INTEX-B mission *Atmos. Chem. Phys.* **9** 5131–53
- [6] Lu Z, Zhang Q and Streets D G 2011 Sulfur dioxide and primary carbonaceous aerosol emissions in China and India, 1996–2010 *Atmos. Chem. Phys.* **11** 9839–64
- [7] Gurney K R, Mendoza D L, Zhou Y, Fischer M L, Miller C C, Geethakumar S and de la Rue du Can S 2009 High resolution fossil fuel combustion CO₂ emission fluxes for the United States *Environ. Sci. Technol.* **43** 5535–41
- [8] Rayner P J, Raupach M R, Paget M, Peylin P and Koffi E 2010 A new global gridded data set of CO₂ emissions from fossil

- fuel combustion: methodology and evaluation *J. Geophys. Res. Atmos.* **115** D19306
- [9] Zhou Y and Gurney K R 2011 Spatial relationships of sector-specific fossil fuel CO₂ emissions in the United States *Glob. Biogeochem. Cycles* **25** GB3002
- [10] Nassar R, Napier-Linton L, Gurney K R, Andres R J, Oda T, Vogel F R and Deng F 2013 Improving the temporal and spatial distribution of CO₂ emissions from global fossil fuel emission data sets *J. Geophys. Res. Atmos.* **118** 917–33
- [11] Oda T and Maksyutov S 2011 A very high-resolution (1 km × 1 km) global fossil fuel CO₂ emission inventory derived using a point source database and satellite observations of nighttime lights *Atmos. Chem. Phys.* **11** 543–56
- [12] Gately C K, Hutyra L R, Wing I S and Brondfield M N 2013 A bottom up approach to on-road CO₂ emissions estimates: improved spatial accuracy and applications for regional planning *Environ. Sci. Technol.* **47** 2423–30
- [13] Gately C K, Hutyra L R and Sue Wing I 2015 Cities, traffic, and CO₂: a multidecadal assessment of trends, drivers, and scaling relationships *Proc. Natl Acad. Sci.* **112** 4999–5004
- [14] Zheng B, Zhang Q, Tong D, Chen C, Hong C, Li M, Geng G, Lei Y, Huo H and He K 2017 Resolution dependence of uncertainties in gridded emission inventories: a case study in Hebei, China *Atmos. Chem. Phys.* **17** 921–33
- [15] Geng G, Zhang Q, Martin R V, Lin J, Huo H, Zheng B, Wang S and He K 2017 Impact of spatial proxies on the representation of bottom-up emission inventories: a satellite-based analysis *Atmos. Chem. Phys.* **17** 4131–45
- [16] Zheng H, Cai S, Wang S, Zhao B, Chang X and Hao J 2019 Development of a unit-based industrial emission inventory in the Beijing–Tianjin–Hebei region and resulting improvement in air quality modeling *Atmos. Chem. Phys.* **19** 3447–62
- [17] Zhou Y, Zhao Y, Mao P, Zhang Q, Zhang J, Qiu L and Yang Y 2017 Development of a high-resolution emission inventory and its evaluation and application through air quality modeling for Jiangsu Province, China *Atmos. Chem. Phys.* **17** 211–33
- [18] Zheng B, Cheng J, Geng G, Wang X, Li M, Shi Q, Qi J, Lei Y, Zhang Q and He K 2021 Mapping anthropogenic emissions in China at 1 km spatial resolution and its application in air quality modeling *Sci. Bull.* **66** 612–20
- [19] Wang Y, Wang J, Zhou M, Henze D K, Ge C and Wang W 2020 Inverse modeling of SO₂ and NO_x emissions over China using multisensor satellite data—part 2: downscaling techniques for air quality analysis and forecasts *Atmos. Chem. Phys.* **20** 6651–70
- [20] Xiong T, Jiang W and Gao W 2016 Current status and prediction of major atmospheric emissions from coal-fired power plants in Shandong Province, China *Atmos. Environ.* **124** 46–52
- [21] Liu F, Zhang Q, Tong D, Zheng B, Li M, Huo H and He K B 2015 High-resolution inventory of technologies, activities, and emissions of coal-fired power plants in China from 1990 to 2010 *Atmos. Chem. Phys.* **15** 13299–317
- [22] Wang K, Tian H, Hua S, Zhu C, Gao J, Xue Y, Hao J, Wang Y and Zhou J 2016 A comprehensive emission inventory of multiple air pollutants from iron and steel industry in China: temporal trends and spatial variation characteristics *Sci. Total Environ.* **559** 7–14
- [23] Qi J, Zheng B, Li M, Yu F, Chen C, Liu F, Zhou X, Yuan J, Zhang Q and He K 2017 A high-resolution air pollutants emission inventory in 2013 for the Beijing–Tianjin–Hebei region, China *Atmos. Environ.* **170** 156–68
- [24] Zhao Y, Xia Y and Zhou Y 2018 Assessment of a high-resolution NO_x emission inventory using satellite observations: a case study of southern Jiangsu, China *Atmos. Environ.* **190** 135–45
- [25] Beirle S, Boersma K F, Platt U, Lawrence M G and Wagner T 2011 Megacity emissions and lifetimes of nitrogen oxides probed from space *Science* **333** 1737–9
- [26] Valin L C, Russell A R and Cohen R C 2013 Variations of OH radical in an urban plume inferred from NO₂ column measurements *Geophys. Res. Lett.* **40** 1856–60
- [27] Fioletov V E, McLinden C A, Krotkov N and Li C 2015 Lifetimes and emissions of SO₂ from point sources estimated from OMI *Geophys. Res. Lett.* **42** 1969–76
- [28] Liu F, Beirle S, Zhang Q, Dörner S, He K and Wagner T 2016 NO_x lifetimes and emissions of cities and power plants in polluted background estimated by satellite observations *Atmos. Chem. Phys.* **16** 5283–98
- [29] McLinden C A, Fioletov V, Shephard M W, Krotkov N, Li C, Martin R V, Moran M D and Joiner J 2016 Space-based detection of missing sulfur dioxide sources of global air pollution *Nat. Geosci.* **9** 496–500
- [30] Liu F, Duncan B N, Krotkov N A, Lamsal L N, Beirle S, Griffin D, McLinden C A, Goldberg D L and Lu Z 2020 A methodology to constrain carbon dioxide emissions from coal-fired power plants using satellite observations of co-emitted nitrogen dioxide *Atmos. Chem. Phys.* **20** 99–116
- [31] Liu F, Beirle S, Zhang Q, van der A R J, Zheng B, Tong D and He K 2017 NO_x emission trends over Chinese cities estimated from OMI observations during 2005–2015 *Atmos. Chem. Phys.* **17** 9261–75
- [32] Veefkind J P et al 2012 TROPOMI on the ESA sentinel-5 precursor: a GMES mission for global observations of the atmospheric composition for climate, air quality and ozone layer applications *Remote Sens. Environ.* **120** 70–83
- [33] Beirle S, Borger C, Dörner S, Li A, Hu Z, Liu F, Wang Y and Wagner T 2019 Pinpointing nitrogen oxide emissions from space *Sci. Adv.* **5** eaax9800
- [34] Goldberg D L, Lu Z, Streets D G, de Foy B, Griffin D, McLinden C A, Lamsal L N, Krotkov N A and Eskes H 2019 Enhanced capabilities of TROPOMI NO₂: estimating NO_x from North American Cities and power plants *Environ. Sci. Technol.* **53** 12594–601
- [35] Li M et al 2017 Anthropogenic emission inventories in China: a review *Nat. Sci. Rev.* **4** 834–66
- [36] Zheng B et al 2018 Trends in China's anthropogenic emissions since 2010 as the consequence of clean air actions *Atmos. Chem. Phys.* **18** 14095–111
- [37] National Bureau of Statistics of People's Republic of China 2017 *China City Statistical Yearbook 2017* (Beijing: China Statistics Press)
- [38] van Geffen J H G M, Eskes H J, Boersma K F, Maasakkers J D and Veefkind J P 2019 TROPOMI ATBD of the total and tropospheric NO₂ data products (S5P-KNMI-L2-0005-RP, Royal Netherlands Meteorological Institute) (available at: <https://sentinel.esa.int/documents/247904/2476257/Sentinel-5P-TROPOMI-ATBD-NO2-data-products>) (accessed 23 April 2020)
- [39] Griffin D et al 2019 High-resolution mapping of nitrogen dioxide with TROPOMI: first results and validation over the Canadian oil sands *Geophys. Res. Lett.* **46** 1049–60
- [40] Wang C, Wang T, Wang P and Rakitin V 2020 Comparison and validation of TROPOMI and OMI NO₂ observations over China *Atmosphere* **11** 636
- [41] Boersma K, Eskes H and Brinksma E 2004 Error analysis for tropospheric NO₂ retrieval from space *J. Geophys. Res.* **109** D04311
- [42] Lorente A et al 2017 Structural uncertainty in air mass factor calculation for NO₂ and HCHO satellite retrievals *Atmos. Meas. Tech.* **10** 759–82
- [43] Lorente A, Boersma K F, Eskes H J, Veefkind J P, Van Geffen J H G M, De Zeeuw M B, Denier van der Gon H A C, Beirle S and Krol M C 2019 Quantification of nitrogen oxides emissions from build-up of pollution over Paris with TROPOMI *Sci. Rep.* **9** 20033
- [44] McLinden C A, Fioletov V, Boersma K F, Kharol S K, Krotkov N, Lamsal L, Makar P A, Martin R V, Veefkind J P and Yang K 2014 Improved satellite retrievals of NO₂ and SO₂ over the Canadian oil sands and comparisons with surface measurements *Atmos. Chem. Phys.* **14** 3637–56

- [45] Van Geffen J, Boersma K F, Eskes H, Sneep M, Ter Linden M, Zara M and Veefkind J P 2020 S5P TROPOMI NO₂ slant column retrieval: method, stability, uncertainties and comparisons with OMI *Atmos. Meas. Tech.* **13** 1315–35
- [46] Boersma K F *et al* 2011 An improved tropospheric NO₂ column retrieval algorithm for the Ozone monitoring instrument *Atmos. Meas. Tech.* **4** 1905–28
- [47] Lu Z, Streets D G, De Foy B, Lamsal L N, Duncan B N and Xing J 2015 Emissions of nitrogen oxides from US urban areas: estimation from Ozone monitoring instrument retrievals for 2005–2014 *Atmos. Chem. Phys.* **15** 10367–83
- [48] Zhao Y *et al* 2015 Advantages of a city-scale emission inventory for urban air quality research and policy: the case of Nanjing, a typical industrial city in the Yangtze River Delta, China *Atmos. Chem. Phys.* **15** 12623–44
- [49] Liu F *et al* 2018 A new global anthropogenic SO₂ emission inventory for the last decade: a mosaic of satellite-derived and bottom-up emissions *Atmos. Chem. Phys.* **18** 16571–86
- [50] Luo J, Han Y, Zhao Y, Liu X, Huang Y, Wang L, Chen K, Tao S, Liu J and Ma J 2020 An inter-comparative evaluation of PKU-FUEL global SO₂ emission inventory *Sci. Total Environ.* **722** 137755